

The CO₂ Abundance in Comets C/2012 K1 (PanSTARRS), C/2012 K5 (LINEAR), and 290P/Jäger as Measured with *Spitzer*

Adam J. McKay^a, Michael S. P. Kelley^b, Anita L. Cochran^a,
Dennis Bodewits^b, Michael A. DiSanti^{c,d}, Neil Dello Russo^e,
Carey M. Lisse^e

^a*University of Texas Austin/McDonald Observatory, 1 University Station, Austin,
TX 78712, (U.S.A.); amckay@astro.as.utexas.edu, anita@astro.as.utexas.edu*

^b*Department of Astronomy, University of Maryland, College Park, MD
20742-2421 (U.S.A.); msk@astro.umd.edu, dennis@astro.umd.edu*

^c*NASA Goddard Center for Astrobiology, NASA GSFC, Mail Stop 690, Greenbelt,
MD 20771 (U.S.A.); Michael.A.Disanti@nasa.gov*

^d*Solar System Exploration Division, Mail Stop 690, Greenbelt, MD 20771 (U.S.A.)*

^e*Johns Hopkins University Applied Physics Laboratory, 11100 Johns Hopkins Rd.,
Laurel, MD, 20723 (U.S.A.); neil.dello.russo@jhuapl.edu, carey.lisse@jhuapl.edu*

Copyright © 2015 Adam J. McKay, Michael S. Kelley, Anita L. Cochran, Dennis Bodewits, Michael A.
DiSanti, Neil Dello Russo, Carey M. Lisse

Number of pages: 31

Number of tables: 6

Number of figures: 7

Proposed Running Head:

CO₂ in Comets PanSTARRS, LINEAR, and Jäger

Please send Editorial Correspondence to:

Adam J. McKay

University of Texas Austin

2512 Speedway, Stop C1402

Austin, TX 78712, USA.

Email: amckay@astro.as.utexas.edu

Phone: (512) 471-6493

ABSTRACT

Carbon dioxide is one of the most abundant ices present in comets and is therefore important for understanding cometary composition and activity. We present analysis of observations of CO₂ and [O I] emission in three comets to measure the CO₂ abundance and evaluate the possibility of employing observations of [O I] emission in comets as a proxy for CO₂. We obtained NIR imaging sensitive to CO₂ of comets C/2012 K1 (PanSTARRS), C/2012 K5 (LINEAR), and 290P/Jäger with the IRAC instrument on *Spitzer*. We acquired observations of [O I] emission in these comets with the ARCES echelle spectrometer mounted on the 3.5-meter telescope at Apache Point Observatory and observations of OH with the *Swift* observatory (PanSTARRS) and with Keck HIRES (Jäger). The CO₂/H₂O ratios derived from the *Spitzer* images are $12.6 \pm 1.3\%$ (PanSTARRS), $28.9 \pm 3.6\%$ (LINEAR), and $31.3 \pm 4.2\%$ (Jäger). These abundances are derived under the assumption that contamination from CO emission is negligible. The CO₂ abundance for PanSTARRS is close to the average abundance measured in comets at similar heliocentric distance to date, while the abundances measured for LINEAR and Jäger are significantly larger than the average abundance. From the coma morphology observed in PanSTARRS and the assumed gas expansion velocity, we derive a rotation period for the nucleus of about 9.2 hours. Comparison of H₂O production rates derived from ARCES and *Swift* data, as well as other observations, suggest the possibility of sublimation from icy grains in the inner coma. We evaluate the possibility that the [O I] emission can be employed as a proxy for CO₂ by comparing CO₂/H₂O ratios inferred from the [O I] lines to those measured directly by *Spitzer*. We find that for PanSTARRS we can reproduce the observed CO₂ abundance to an accuracy of $\sim 20\%$. For LINEAR and Jäger,

we were only able to obtain upper limits on the CO₂ abundance inferred from the [O I] lines. These upper limits are consistent with the CO₂ abundances measured by *Spitzer*.

Keywords: Comets; Comets, Coma; Comets, Composition

1 Introduction

The abundances of CO and CO₂ in comets may either reflect thermal evolution (Belton and Melosh, 2009) or formation conditions (A’Hearn et al., 2012), with the distinct possibility that both evolution and formation conditions play a major role. The formation of CO₂ likely occurs via grain surface interactions of OH and CO, though this reaction is not completely understood (e.g. Garrod and Pauly, 2011; Noble et al., 2011). Another possible pathway is direct oxidation of CO on grain surfaces (Minissale et al., 2013). In either case, this would imply that CO₂ forms from destruction of CO and hence, if these reactions are efficient (i.e. most CO in the protosolar disk is converted to CO₂ via these reactions), on average CO₂ should be more abundant than CO in comets. This abundance pattern could also be caused by thermal evolution due to CO being more volatile than CO₂ or the protosolar disk inherently having a CO₂/CO ratio greater than unity in the comet forming region that was inherited from the ISM. In the case of evolution there should be observed trends in CO/CO₂ ratios as a function of the dynamical history of the comet. Definitive evidence for any such trend has not been observed (A’Hearn et al., 2012), though it is possible that not enough comets have been observed for any trend that is present to become apparent. Therefore, knowledge of the CO and CO₂ abundances in comets is paramount for creating a complete picture of cometary composition and differentiating between the effect of formation conditions and subsequent thermal evolution on cometary composition.

However, the lack of a permanent dipole moment for CO₂ means it is best observed directly through its vibrational transitions at infrared wavelengths

(CO₂ also has electronic transitions, but these are very weak and have never been observed astronomically). The only successful direct observations of CO₂ in comets have been of its ν_3 vibrational band at 4.26 μm , which is heavily obscured by the presence of telluric CO₂ and therefore cannot be observed from the ground. Before 2004, the CO₂ abundance had been measured for only a few comets (Combes et al., 1988; Crovisier, 1997), with many more observations becoming available over the last 10 years thanks to space-borne assets. Observations of CO₂ in comets by *Spitzer* (Pittichová et al., 2008; Reach et al., 2009, 2013), AKARI (Ootsubo et al., 2010, 2012), *WISE* (Bauer et al., 2011, 2012; Stevenson et al., 2015; Bauer et al., 2015), and the Deep Impact spacecraft (Feaga et al., 2007; A’Hearn et al., 2011; Feaga et al., 2014), have revealed that CO₂ is the second most abundant gas present in most cometary comae (behind H₂O). This may favor a mechanism where the CO₂ present in comets was formed via reactions that destroy CO and also possibly favor the idea that the measured abundances are indeed primordial. Observations of Cameron band emission of CO with *HST* have also been employed as a proxy for CO₂ (Weaver et al., 1994). However, Cameron band emission has a significant contribution from electron impact excitation of CO, which complicates derivation of the CO₂ abundance (Bhardwaj and Raghuram, 2011).

The only facilities that can currently observe CO₂ in comets are the *Spitzer* Space Telescope and the *WISE* spacecraft (directly in the IR), as well as *HST* (through Cameron band emission.) However, as these are all space-borne facilities, the observing time available is limited. In addition, *Spitzer* and *WISE* all have very stringent elongation requirements, meaning many objects go unobserved (even though *WISE/NEOWISE* is a survey, it only observes at 90° elongation, meaning observations of comets are serendipitous and can-

not be planned for detailed study of a particular comet). The James Webb Space Telescope (JWST) is expected to supercede the capabilities provided by *Spitzer* and *WISE* for cometary science (Kelley et al., 2015), but JWST observing time for comets may be limited. Ground-based observations are in general more accessible than space-borne assets, allowing for more detailed study of a larger number of objects. Therefore, establishment of an indirect, ground-based measure of CO₂ abundances in comets is vital in order to provide the number of measurements needed for further interpretation of comet origin and evolution.

As atomic oxygen is a photodissociation product of CO₂, observations of the forbidden oxygen lines at 5577, 6300, and 6364 Å can serve as a viable proxy. These forbidden lines are fairly bright features in cometary spectra and can be readily observed in moderately bright comets (V=10) with medium aperture telescopes (2-3 meter class) (Capria et al., 2005; Cochran, 2008; Decock et al., 2013; McKay et al., 2015, and references therein). However, the photochemistry of O I release from CO₂ photodissociation, as well as from its other primary parents H₂O and CO, is still poorly understood, and limits the usefulness of O I as a reliable proxy (McKay et al., 2013; Decock et al., 2013). However, if independent, contemporaneous measurements of H₂O, CO₂, CO, and O I are available, it is possible to employ comets as a “laboratory” to constrain the relevant photochemistry.

We present analysis of *Spitzer* Infrared Array Camera (IRAC) imaging of comets C/2012 K1 (PanSTARRS), C/2012 K5 (LINEAR), and 290P/Jäger (hereafter PanSTARRS, LINEAR, and Jäger, respectively), which we employ to measure the CO₂ production rate in each comet. We also present high

resolution optical spectroscopy of these comets in an effort to observe the [O I] emission and therefore constrain the photochemistry responsible for the release of O I into the coma. In section 2 we describe our observations and reduction and analysis procedures. Section 3 presents our CO₂ production rates and [O I] line measurements, and a comparison of the CO₂ abundances inferred from the [O I] emission and the abundances measured with *Spitzer*. In section 4 we discuss how the measured CO₂ production rates fit in with the growing sample of CO₂ observations in comets, as well as the implications of our results for the photochemistry of O I release and the ability to use [O I] observations as a proxy for CO₂. Section 5 summarizes our conclusions.

2 Observations and Data Analysis

2.1 Observations

We obtained NIR images at 3.6 and 4.5 μm for studying CO₂ using the IRAC instrument on *Spitzer* (Werner et al., 2004; Fazio et al., 2004), while we obtained optical spectra for studying atomic oxygen with the ARCES echelle spectrometer mounted on the Astrophysical Research Consortium 3.5-m telescope at Apache Point Observatory (APO) in Sunspot, New Mexico. We also obtained optical spectra of Jäger with the HIRES instrument mounted on Keck I and imaging of PanSTARRS with the *Swift* spacecraft to measure the OH production rate, which gives us a measure of the H₂O production rate.

2.1.1 CO₂ - *Spitzer* IRAC

As *Spitzer* is well into its post-cryogenic mission, IRAC presently observes in two pass bands: one centered at 3.6 μm and the other at 4.5 μm . Both filters have broad wavelength coverage, with bandwidths of 0.8 and 1.0 μm , respectively. The 4.5 μm band is very useful for measuring the CO₂ abundances in comets, as this pass band includes the ν_3 transition at 4.26 μm . It also contains the $\nu(1-0)$ band of CO at 4.7 μm , but in 15 out of 17 comets in the AKARI survey (Ootsubo et al., 2012), the CO₂ feature was at least 10 times brighter than the CO feature, and so CO₂ is typically the dominant gas emission feature in the IRAC 4.5 μm band. This is due to the fluorescence efficiency of CO₂ being approximately an order of magnitude larger than that for CO, while the CO abundance in comets is typically equal to or less than the CO₂ abundance. While this is true for most comets, there are examples, such as C/2006 W3 (Christensen) and 29P/Schwassman-Wachmann 1, where CO emission contributes significantly (more than 20%) to the 4.5 μm band flux (Ootsubo et al., 2012; Reach et al., 2013).

We supply details of our observations in Table 1. The IRAC array is a 256 x 256 pixel InSb array, covering a 5' x 5' region on the sky. We performed observations of each comet field several days after each cometary observation in order to image the field without the comet in it. These observations are termed “shadow observations” and provide a measurement of the background to be subtracted from the cometary images. We observed each comet in high dynamic range mode. This entailed obtaining exposures with both short and long exposure times in order to avoid saturation of the inner coma, while still keeping high signal-to-noise ratio (SNR) in the fainter outer coma (details of

the exposure times used are given in Table 1). Observing in high dynamic range mode also helps protect against saturation due to bright field stars. For these observations no pixels were saturated in the longest exposure times, therefore we performed analysis on the longest exposure time images for optimal SNR.

For each comet, we combined all images of the same exposure time using the MOPEX software (Makovoz and Khan, 2005). This process creates a mosaic in the rest frame of the comet from the individual images, averaging overlapping data together, but ignoring cosmic rays and bad pixels. Two mosaics are created: one for the comet data, the other for the shadow (background) data. We subtracted the shadow mosaic from the comet mosaic to remove the background. This includes zodiacal light and celestial sources.

After the mosaic images were created and the sky background was separated, the next step was to remove the dust contribution from the $4.5 \mu\text{m}$ band flux, isolating the gas emission. We accomplished this via the following method. First we split the $4.5 \mu\text{m}$ band image into wedges centered on the optocenter of the comet (for PanSTARRS, this consisted of 20 wedges, while for Jäger and LINEAR the best results were derived assuming spherical symmetry, i.e. no splitting of the images into wedges was applied). We then fit the $4.5 \mu\text{m}$ band image morphology in each wedge (or in the case of LINEAR and Jäger, the whole image) to a model consisting of a $1/\rho$ profile (to approximate the gas) plus the $3.6 \mu\text{m}$ band image (indicative of the dust). Both the $1/\rho$ profile (i.e. gas model) and $3.6 \mu\text{m}$ band fluxes were allowed to be multiplied by a scale factor. The gas scale factor was allowed to vary from wedge to wedge, but the

scaling factor for the 3.6 μm band was forced to be the same for all wedges. The key parameter we retrieved from this modelling is the 3.6 μm band scale factor. Lastly, we multiplied the 3.6 μm band image by the retrieved scale factor and subtracted the scaled 3.6 μm band image from the 4.5 μm band image to obtain a dust-subtracted image.

From the dust-subtracted image, we measured the flux for apertures ranging from 6-60 pixels (7-70") in radius. We converted the broadband photometry to CO₂ line fluxes following the IRAC data handbook (Laine, 2015). The line fluxes were then used to calculate average column densities inside each aperture employing fluorescence efficiencies from Crovisier and Encrenaz (1983). Then the production rate Q is given by

$$Q = \langle N \rangle v d \quad (1)$$

where $\langle N \rangle$ is the average column density in the photometric aperture, v is the expansion velocity, and d is the projected diameter of the photometric aperture. We assume an expansion velocity of the coma following Tseng et al. (2007):

$$v = 0.96 R_h^{-0.44} \quad (2)$$

where R_h denotes the heliocentric distance in AU of the comet and the derived velocity is in km s^{-1} . This approach assumes a negligible effect of photodissociation on the spatial profile in the photometric aperture, but as our apertures are < 10% of the CO₂ scale length, this approximation is justified. We calculated production rates for a variety of aperture sizes to quantify any trends in

derived production rates with aperture size. We find that small trends with aperture size are present, which may be due to residual dust, structure in the gas coma (i.e., the assumed $1/\rho$ relation for the gas surface brightness profile is violated), and/or the difference between the 3.6 and 4.5 μm point-spread functions. Residual dust may be present due to color variations in the coma. We prefer to keep our approach simple, and refrain from using additional free-parameters and assumptions to model these deviations. The uncertainties adopted for the CO_2 production rates are either derived from the 3.6 μm model scale factor uncertainties (LINEAR and Jäger), or from the standard deviation of the derived production rates for all apertures (PanSTARRS), whichever is larger.

To enhance structures in the coma morphology, we divided each image by a $1/\rho$ profile, where ρ is the projected distance from the optocenter. A $1/\rho$ profile is what is expected for a coma in steady state expansion. Any deviations from this theoretical spatial profile are enhanced in the resulting image, allowing studies of the coma morphology to be performed.

2.2 *O I - ARCES*

ARCES is a cross-dispersed echelle spectrometer, providing a spectral resolution of $R \equiv \frac{\lambda}{\Delta\lambda} = 31,500$ and a spectral range of 3500-10,000 \AA with no interorder gaps. This large, uninterrupted spectral range allows for simultaneous observations of all three oxygen lines. More specifics for this instrument are discussed elsewhere (Wang et al., 2003).

The observation dates and geometries are described in Table 2. All nights were photometric, meaning absolute flux calibration of the spectra was possible. We used an ephemeris generated from JPL Horizons for non-sidereal tracking. Guiding was accomplished using a boresight technique, which utilizes optocenter flux that falls outside the slit to keep the slit on the optocenter. We observed a G2V star, a fast rotating ($v\sin(i) > 150 \text{ km s}^{-1}$) O, B, or A star, and a flux standard for calibration of the comet spectra. The calibration stars used for each observation date are given in Table 2. We obtained spectra of a quartz lamp for flat fielding and acquired spectra of a ThAr lamp for wavelength calibration.

Spectra were extracted and calibrated using Image Reduction and Analysis Facility (IRAF) scripts that perform bias subtraction, cosmic ray removal, flat fielding, and wavelength calibration. We employed the fast-rotator spectrum to remove telluric features, the flux standard spectrum to convert from counts to physical units, and the solar analog spectrum to remove Fraunhofer lines. We assumed an exponential extinction law and extinction coefficients for APO when flux calibrating the cometary spectra. More details of our reduction procedures can be found in McKay et al. (2015) and references therein.

Because of the small size of the ARCES slit, it is necessary to obtain an estimate of the slit losses to achieve an accurate flux calibration. We find the transmittance through the slit by performing aperture photometry on the slit viewer images as described in McKay et al. (2014). This introduces a 10% un-

certainty in our absolute flux calibration.

The O I lines are also present as a telluric emission feature, meaning a combination of high spectral resolution and large geocentric velocity (and therefore large Doppler shift) is needed to separate the cometary line from the telluric feature. For all observations the telluric and cometary lines are well separated. We fit the line profiles using the Gaussian-fitting method described in McKay et al. (2012). Emission from the C₂ Δv=-1 Swan band can also contaminate the cometary 5577 Å feature (e.g. Decock et al., 2013). However, there is no trace of C₂ emission in any of the observed comets in the wavelength region surrounding the 5577 Å feature. Therefore we consider any contamination from C₂ negligible. The 6300 Å and 6364 Å lines are both transitions from the ¹D to the ³P ground state, therefore the flux ratio reflects the branching ratio for these transitions of 3.0. This means that the flux ratio of these lines is independent of the coma physics, and the expected value of 3.0 is well established by both theory and observation (Sharpee and Slanger, 2006; Cochran and Cochran, 2001; Cochran, 2008; McKay et al., 2012, 2013; Decock et al., 2013). As a check of our analysis procedures, we confirmed that we reproduced this ratio before proceeding with further analysis.

With the measured line fluxes, we calculate the oxygen line ratio, defined as

$$R = \frac{I_{5577}}{I_{6300} + I_{6364}} \tag{3}$$

where I_y denotes the flux of line y . The CO₂/H₂O ratio can be inferred from the oxygen line ratio using the following relation (McKay et al., 2012;

Decock et al., 2013):

$$\frac{N_{CO_2}}{N_{H_2O}} = \frac{RW_{H_2O}^{red} - W_{H_2O}^{green} - W_{CO}^{green} \frac{N_{CO}}{N_{H_2O}} + RW_{CO}^{red} \frac{N_{CO}}{N_{H_2O}}}{W_{CO_2}^{green} - RW_{CO_2}^{red}} \quad (4)$$

where N is column density and R is the oxygen line ratio. The release rate W is defined as

$$W \equiv \tau^{-1} \alpha \beta \quad (5)$$

where τ represents the photodissociative lifetime of the parent molecule, α is the yield into the excited state of interest, and β represents the branching ratio for a given line out of a certain excited state. This relation is derived by noting that the line flux contributed from each species is given by the product of column density N and release rate W , substituting this into Eq. 3 and solving for $\frac{N_{CO_2}}{N_{H_2O}}$ (see McKay et al. (2012) for more details). We ignore the contribution of more complex oxygen-bearing molecules like H_2CO and CH_3OH as these species are less abundant than H_2O , CO_2 , and CO and release oxygen through a multi-step process, making them very inefficient at contributing to the O I population. If the contribution of CO photodissociation to the O I population is also considered negligible (Raghuram and Bhardwaj, 2014), Eq. 4 simplifies to (McKay et al., 2013):

$$\frac{N_{CO_2}}{N_{H_2O}} = \frac{RW_{H_2O}^{red} - W_{H_2O}^{green}}{W_{CO_2}^{green} - RW_{CO_2}^{red}} \quad (6)$$

The results of Eq. 4 and 6 are independent of heliocentric distance. For small fields of view, the column density ratio reflects the production rate ratio (see McKay et al., 2015, and references therein for more details).

We performed additional analysis accounting for preferential collisional quench-

ing of ^1D atoms (responsible for the 6300 Å and 6364 Å lines) as compared to ^1S atoms (responsible for the 5577 Å line), which can be important for small fields of view or high production rates (Bhardwaj and Raghuram, 2012; Raghuram and Bhardwaj, 2014; Decock et al., 2015). The oxygen line ratio employed in Eqs. 4 and 6 assumes the ratio was calculated using 6300 Å and 6364 Å line intensities that are unaffected by collisional quenching. Since this may not be the case, the observed 6300 Å and 6364 Å line intensities need to be increased to account for the ^1D atoms that were de-excited through collisions and so do not contribute to the 6300 Å and 6364 Å line intensities. In order to account for this, we need to model the number density of the dominant collisional partner, H_2O . Therefore an estimate of the H_2O production rate is needed.

We determined H_2O production rates from our [O I]6300 Å line observations by employing algorithms based on those used in Morgenthaler et al. (2007) and McKay et al. (2012), which involves a Haser model modified to emulate the more physical vectorial model. With an H_2O production rate in hand, we estimate the percentage of atoms lost to collisional quenching by employing the algorithms mentioned above to estimate the expected [O I]6300 Å flux without collisional quenching. The correction factor is then simply the expected flux without quenching divided by the observed flux. More details concerning this method are presented in McKay et al. (2015).

2.3 OH-Swift and HIRES

The *Swift* telescope (Gehrels et al., 2004) observed PanSTARRS on May 6 and 7, 2014 at R=2.04 AU from the Sun. We employed the UVOT instrument (Mason et al., 2004; Roming et al., 2005) to obtain photometry of the comet. UVOT’s broadband filters provide a measure of the comet’s water and dust production rates (Bodewits et al., 2014). We obtained photometry using broadband V (central λ 5468 Å, FWHM 750 Å) and UVW1 (central λ 2600 Å, FWHM 700 Å) filters. We used the UVW1 filter to detect OH emission and the V-band filter to remove the contribution of continuum in the UVW1 filter. We scaled the V-band flux to the UVW1 filter by assuming the reflected dust continuum is a solar spectrum with no reddening. We note that there is likely some contamination from C₂ Swan band emission in the V-band filter. Correcting for the filter transmission at the relevant wavelengths, the measured fluxes can be converted into column densities using heliocentric distance and velocity dependent fluorescent efficiencies (Schleicher and A’Hearn, 1988). To derive water production rates, we compare the measured OH content of the coma with an OH distribution calculated using the vectorial model (Festou, 1981; Combi et al., 2004). Most of the uncertainty in the derived production rates is introduced from the modeling, with a negligible contribution coming from photon noise. We measured fluxes in several aperture sizes, and adopt the standard deviation of the derived production rates as our 1-sigma uncertainty.

For Jäger, we obtained observations of OH with the HIRES instrument (Vogt et al., 1994) on Keck I in January 2014. The HIRESb configuration provides observations of the OH $\Delta v=0$ band at 3080 Å. We utilized the 0.86 × 7.0” slit. Observing procedures, reduction, and analysis of the data are very similar

to ARCES. For these observations the Full Moon was only six degrees away from Jäger, meaning a large amount of scattered moonlight was present in the spectra. The additional strong continuum introduced from the scattered moonlight dominates the Poisson noise in the spectra and was difficult to remove completely. We extract the band flux using a spectral fitting model very similar to that presented in McKay et al. (2014). This flux is then converted to an H₂O production rate using a Haser model that has been modified to emulate the vectorial model (see McKay et al. (2014) for more details) and the fluorescence efficiency from Schleicher and A’Hearn (1988). The scale lengths for the Haser model are adopted from Cochran and Schleicher (1993).

3 Results

We provide measured fluxes for CO₂ from our *Spitzer* observations (including 3.6 μ m image scale factors, see section 2.1.1), [O I]6300 Å emission from our ARCES observations, and OH from our *Swift* and Keck HIRES observations in Table 3. All uncertainties are 1-sigma.

3.1 H₂O Production Rates and Collisional Quenching Factors

We show a spectrum of Jäger showing the OH lines (from which we derived the H₂O production rate) in Fig. 1. As discussed in Section 2.3, the noisy background is largely due to scattered sunlight from the Full Moon. We present our H₂O production rates and collisional quenching correction factors in Table 4. A small collisional quenching factor is required for the PanSTARRS data, while for LINEAR and Jäger the effect is negligible due to their much

smaller H₂O production rates. As we are using [O I]6300 emission to derive H₂O production rates, it is desirable to have independent production rates determined via other methods to confirm that there is no systematic error being introduced by employing [O I] emission.

PanSTARRS was by far the brightest of these comets, and therefore several other measurements of the H₂O production rate are available. Gibb et al. (private communication) measured the H₂O production rate with NIRSPEC, and their value is consistent with our value of $(4.35 \pm 0.44) \times 10^{28}$ molecules s⁻¹ derived from [O I]6300 emission to within $\sim 10\%$. From the *Swift*/UVOT observations we derived a water production rate of $(9.5 \pm 0.8) \times 10^{28}$ molecules s⁻¹ in apertures between 50-200 arcsec (5.3×10^4 - 2.1×10^5 km at the comet). Analysis of OH observations by Knight and Schleicher (2014) and of Lyman- α emission by Combi et al. (2014) derive similar production rates. One possibility for the discrepancy is that the H₂O production rate depends on rotational phase of the nucleus. However, as our [O I]6300 observations and the NIRSPEC observations occurred on completely different nights, it is unlikely that both would have sampled the same part of the rotational variation. In addition, this would imply that the observations of Schleicher, Combi et al. (2014), and our *Swift* observations (which also occurred on different dates) would have all sampled the same part of the rotational variation that was also distinct from that sampled by our [O I]6300 observations and the NIRSPEC observations. A more likely possibility is related to the fields of view (FOV) of the different telescope/instrument combinations employed. Our [O I]6300 observations and the NIRSPEC observations of Gibb et al. both employed narrow slits (projected FOV at the comet on the order of several thousand km), while the *Swift*, Combi et al. (2014), and Schleicher observations all used much larger

FOV, on the order of tens to hundreds of thousands of kilometers. A similar dependence of derived H₂O production rates with FOV was observed for C/2009 P1 (Garradd) (Combi et al., 2013; Bodewits et al., 2014; DiSanti et al., 2014; Feaga et al., 2014; McKay et al., 2015). This was interpreted as an extended source of icy grains that sublimated outside the FOV of slit-based spectroscopic measurements, but within the FOV of narrow band imaging observations. A similar phenomenon could be applicable to PanSTARRS. This raises the question of which H₂O production rate is appropriate to adopt for comparison to our [O I] observations. As our O I observations have a small FOV, we will employ the H₂O production rate derived from small FOV observations for the analysis throughout the rest of this paper (but see Section 4.1 for more discussion on how this affects comparison to other observations).

There are no other sources of H₂O production rates available for Jäger or LINEAR. We have observations of OH for Jäger, but these are two months after the [O I] observations. However, as the collisional quenching was determined to be negligible for LINEAR and Jäger, any systematic uncertainties in our H₂O production rate due to employing [O I]6300 emission to obtain an H₂O production rate will have a negligible effect on our CO₂/H₂O ratios inferred from the oxygen line ratio.

It is possible that systematic uncertainties in the H₂O production rate will also affect the *Spitzer*-derived CO₂/H₂O ratios. However, as discussed above, independent direct observations of H₂O using NIRSPEC are consistent with our adopted H₂O production rate for PanSTARRS. For Jäger, our preferred H₂O production rate for comparison to the *Spitzer* measurement of CO₂ is

from HIRES using OH due to this observation being more contemporaneous with the *Spitzer* observations than the [O I] observations. LINEAR has no independent measure of the H₂O production rate, but the agreement of H₂O production rates derived for PanSTARRS and Jäger to other methods gives us confidence that our derived H₂O production rate for LINEAR is accurate to the quoted uncertainties.

3.2 CO₂ Production Rates and Coma Morphology

In Fig. 2 we show the *Spitzer* IRAC images of PanSTARRS, LINEAR, and Jäger. PanSTARRS was by far the brightest of the three comets observed, as is evident in the quality of the images. For PanSTARRS even in the raw mosaics (i.e. no image enhancement or dust subtraction), it is evident that in the 4.5 μm image there is a diffuse, extended emission that is not present in the 3.6 μm image and is likely due to CO₂ or CO gas. We present the dust-subtracted images in Fig. 3.

We present the derived CO₂ production rates and CO₂/H₂O ratios under the assumption of negligible CO emission in Table 4. The quoted uncertainties include only stochastic noise and uncertainties with the modeling used to isolate the gaseous emission, and do not include any systematic error associated with any possible CO emission. While in principal there is both emission from CO₂ and CO in the 4.5 μm image, NIRSPEC observations by Gibbs et al. (private communication) constrain the CO/H₂O ratio for PanSTARRS at $\sim 3\%$. At this abundance the contribution of CO emission to the 4.5 μm flux is minimal (on the order of 3%) and we can assume, within our uncertainties,

that all the gas emission we observe is due to CO₂ in this case. There are no independent measurements of CO available in Jäger or LINEAR, meaning in these cases our CO₂ production rates could in fact be upper limits. However, for most comets in the AKARI survey (Ootsubo et al., 2012), the CO emission was much weaker than that from CO₂. Therefore in general it is likely that our CO₂ production rates for Jäger and LINEAR are not contaminated by CO emission, but without direct, independent observations of CO we cannot be certain. However, even with a CO/H₂O ratio as high as $\sim 30\%$ (higher than any comet in the AKARI survey except C/2006 W3 (Christensen) and 29P/Schwassman-Wachmann 1 and higher than all comets observed from ground-based IR spectroscopy (Mumma and Charnley, 2011) except C/2009 P1 (Garradd) (Feaga et al., 2014; McKay et al., 2015)), the derived CO₂/H₂O abundances from the *Spitzer* observations of LINEAR and Jäger only drop to about 23% and 27%, respectively. Therefore, for our derived CO₂ abundances to change significantly, LINEAR and Jäger would have to have extremely abnormal CO/H₂O ratios ($> 100\%$, only observed for comets C/2006 W3 (Christensen), 29P/Schwassman-Wachmann 1, and C/1995 O1 (Hale-Bopp) (Biver et al., 2002) at larger heliocentric distances than the comets studied here) as compared to the observed sample of comets (Ootsubo et al., 2012; A’Hearn et al., 2012). For LINEAR, the presence of gas emission in the 4.5 μm images was not obvious and the detection of CO₂ is sensitive to model assumptions employed to isolate the gas emission. Therefore in this case our derived CO₂ production rate may be better interpreted as an upper limit.

In Fig. 4, the top row shows (from left to right) the 3.6 μm , 4.5 μm , and dust-subtracted images of PanSTARRS. The bottom row is the same, except

these images have been divided by a $1/\rho$ profile to show coma features. Figs. 5 and 6 show the analogous figures for LINEAR and Jäger, respectively. All the images show a clear tail excess. Even the gas images show some residual tails, suggesting that the dust subtraction is not perfect. For PanSTARRS, a spiral shape is visible in the $4.5 \mu\text{m}$ image and the gas image, but is not present in the $3.6 \mu\text{m}$ image. This is likely the manifestation of a CO_2 jet. Observations of the CN morphology also show this spiral structure, while observations of the dust through R-band imaging do not (Knight and Schleicher, 2014). The *Swift* imaging of OH also does not show any discernible morphology. This may indicate that the OH (and its parent H_2O) is released from the nucleus in a manner that is different from the CN parent and CO_2 , but this could also be due to any morphology that is present being blurred by the random direction of the velocity that OH receives after photodissociation of H_2O .

We can use the separation between arcs of the spiral morphology to obtain an estimate of the rotation period. To determine the positions of the arcs, we measured the total flux in concentric annuli centered on the comet photocenter. Annuli containing the arcs will have higher flux than adjacent annuli. To increase the accuracy of the derived arc positions, we then fit the spatial distribution of flux within the annuli containing an arc with a Gaussian function plus constant background. We derive mean peak centers at 25.1 ± 0.3 and 48.3 ± 1.0 pixels from the optocenter, corresponding to 26700 ± 300 and 51200 ± 1100 km. These positions predict additional arcs should be present at 1.9 and 71.5 pixels from the optocenter. The 1.9 pixel offset is too close to the comet to resolve, but the surface brightness profile does seem to be peaked quite close to the center. The 71.5 pixel peak is not apparent, but may

be too diffuse to resolve in our data. Assuming an expansion speed of 0.74 km/s in the plane of the sky (derived from the Tseng et al. (2007) relation, see Section 2.1), the apparent period is 9.2 ± 0.4 hr, which we identify as a candidate rotation period for the nucleus. The CN morphology observed by Knight and Schleicher (2014) is consistent with this rotation period, but their analysis does not provide a definitive value.

The spatial profile for all the LINEAR images is very symmetric and shows no notable features. The Jäger dust-subtracted image shows possible asymmetry to the bottom of the image, but no obvious coma structures such as observed for PanSTARRS that could be used to derive a rotation period are present.

3.3 *O I Line Ratios and Inferred CO₂ Abundances*

We present our oxygen line ratio measurements and 3-sigma upper limits in Table 5. Unfortunately, LINEAR and Jäger were not bright enough for detection of the [O I]5577 Å line, and the upper limits are not particularly constraining. However, PanSTARRS was much brighter and we have a firm detection of the [O I]5577 Å line, as shown in Fig. 7.

We derive CO₂/H₂O ratios from our oxygen line ratios (or 3-sigma upper limits in the case of LINEAR and Jäger) using release rates from Bhardwaj and Raghuram (2012) and McKay et al. (2015). We summarize our CO₂ abundances directly measured by *Spitzer* and our inferred CO₂ abundances from our oxygen line

observations in Table 5. The specific values for the release rates are given in Table 6. The rates from Bhardwaj and Raghuram (2012) are derived from a photochemical model of a cometary coma, while the empirical rates from McKay et al. (2015) are rates that are able to reproduce the $\text{CO}_2/\text{H}_2\text{O}$ ratio determined by Feaga et al. (2014) for comet C/2009 P1 (Garradd). The difference between empirical release rates A and B from McKay et al. (2015) is a factor of 1.5 in the CO_2 release rates that accounts for differences in the $\text{CO}/\text{H}_2\text{O}$ abundance in Garradd measured by McKay et al. (2015) and Feaga et al. (2014). For PanSTARRS, we used Eq. 4, which includes the contribution of CO, with a $\text{CO}/\text{H}_2\text{O}$ ratio of $\sim 3\%$ (Gibbs et al. private communication). As no independent measure of the CO abundance is available for Jäger or LINEAR, we applied Eq. 6, which assumes no contribution to the O I population from CO. If the contribution of CO is significant, this would not affect our upper limit, since including a contribution from CO only lowers the inferred upper limit on CO_2 . Therefore our derived upper limits are true upper limits.

Using release rates from Bhardwaj and Raghuram (2012), we infer a $\text{CO}_2/\text{H}_2\text{O}$ ratio of $\sim 4\%$ for PanSTARRS, while the abundance measured by *Spitzer* is approximately 12%. The empirical release rates from McKay et al. (2015) reproduce the $\text{CO}_2/\text{H}_2\text{O}$ ratio to better accuracy, predicting a $\text{CO}_2/\text{H}_2\text{O}$ ratio of $\sim 10\%$ (release rates A) or $\sim 14\%$ (release rates B). The upper limits inferred for Jäger and LINEAR using the McKay et al. (2015) release rates are consistent with the values measured by *Spitzer*, but do not provide further constraints on their accuracy. The upper limit inferred for LINEAR using release rates from Bhardwaj and Raghuram (2012) may be inconsistent with the *Spitzer* result (see section 4.2), but the Jäger results are consistent with

the Bhardwaj and Raghuram (2012) release rates.

4 Discussion

4.1 CO_2 Abundances

The $\text{CO}_2/\text{H}_2\text{O}$ ratio of 12% measured for PanSTARRS is slightly lower than the mean of the AKARI survey of comets measured at heliocentric distances of less than 2.5 AU (i.e. inside the canonical water sublimation line where sublimation rates of H_2O , CO_2 , and CO do not vary much with respect to each other (e.g. Meech and Svoren, 2004)), which is approximately 17% (Ootsubo et al., 2012), but is well within the spread of values observed in comets at similar heliocentric distance to date. The observed CO_2 abundances of 29% and 31% for LINEAR and Jäger, respectively, are higher than any comet observed by AKARI within 2.5 AU from the Sun. However, these values are close to the mean value of 30% found by Reach et al. (2013), although this data set has much more scatter than the AKARI survey.

As both LINEAR (1.6 AU) and Jäger (2.2 AU) were observed at heliocentric distances less than 3 AU, sublimation effects are not likely responsible for these high abundances (Meech and Svoren, 2004). One possibility is that since AKARI observed over a much larger FOV ($1' \times 1'$) than our narrow slit observations, the AKARI observations were sensitive to any extended sources of H_2O that may have been present around the comets in their survey. If an extended source of water was present in Jäger and LINEAR, this would

have resulted in larger derived H₂O production rates and therefore smaller CO₂/H₂O ratios than would have been measured using H₂O production rates from narrow slit observations such as ours. Therefore if we had used an observational set up similar to AKARI with a large FOV to derive H₂O production rates, our derived CO₂/H₂O ratios might have been lower, bringing the measured abundances for LINEAR and Jäger closer to the mean value derived from AKARI. A similar effect is expected for the Reach et al. (2013) sample, as they adopted H₂O production rates from wide field OH imaging. However, without any data indicating the magnitude of an extended source of H₂O production around LINEAR and Jäger, we cannot evaluate this possibility further. Another caveat to consider is the possibility that CO emission is contributing to *Spitzer's* 4.5 μm filter, meaning the CO₂ production rates are in fact lower than presented here. However, as discussed in Section 3.2, this is not likely, as an abnormally large CO abundance is required to change the derived CO₂/H₂O ratio significantly. As mentioned in section 3.2, we cannot rule out the possibility that our detection of CO₂ in LINEAR is better interpreted as an upper limit, in which case its CO₂ abundance would be more typical.

This study, while only adding three new comets to the sample, is consistent with the findings of previous CO₂ surveys in comets that the average CO₂ abundance in comets is about 15-30%, higher than previously thought (Ootsubo et al., 2012; Reach et al., 2013). Only one of our comets has a measurement of the CO abundance (PanSTARRS), and the preliminary CO abundance in this comet derived by Gibbs et al. (private communication) is much less than the CO₂ abundance, consistent with the idea that the formation of CO₂ via grain-

surface reactions involving CO is a viable pathway for CO₂ formation in the protosolar disk. With no observations of CO in LINEAR or Jäger available, we cannot reach any conclusions on the CO/CO₂ ratio in those comets.

4.2 Accuracy of O I as a Proxy for CO₂

Using our *Spitzer* observations, we were able to compare actual CO₂ abundances for these comets to CO₂ abundances inferred using observations of the oxygen line ratio. For PanSTARRS, the Bhardwaj and Raghuram (2012) release rates underestimate the CO₂ abundance by about a factor of three. A similar discrepancy was found for C/2009 P1 (Garradd) (McKay et al., 2015). The upper limits inferred from the oxygen line ratio for Jäger are not particularly constraining, as all three sets of release rates provide upper limits consistent with the *Spitzer* measurements. However, for LINEAR the upper limit on CO₂/H₂O using the Bhardwaj and Raghuram (2012) release rates is similar to the value measured by *Spitzer*. While not conclusive, this suggests that we should have been able to detect the [O I]5577 Å line in this comet, which we did not. However, a lack of knowledge of the CO abundance and the quality of the data prevent us from making a firm conclusion. Therefore there is suggestive (but not conclusive) evidence that the Bhardwaj and Raghuram (2012) release rates do not reproduce the LINEAR observations.

The empirical release rates from McKay et al. (2015) also reproduce the CO₂ abundance observed in comet Garradd (by definition, as this was a requirement in the derivation of these release rates; the two sets of release rates correspond to different values of the CO/H₂O ratio used in Eq. 4). The ability of these

release rates to reproduce the CO₂ abundance in PanSTARRS to within an accuracy of 20% is encouraging, but the lack of detections of the [O I]5577 line in Jäger and LINEAR prevent further evaluation. The empirical release rates B seem to reproduce the CO₂ abundance in PanSTARRS more accurately than the release rates A. More simultaneous observations of CO₂ and the oxygen line ratios in comets are needed to further evaluate this method, and specifically the release rates proposed by McKay et al. (2015).

It is important to stress that the release rates from McKay et al. (2015) are strictly empirical. They seem to satisfactorily reproduce current observations, but there is no physical explanation for why they are different from those derived using photochemical models, such as those presented in Bhardwaj and Raghuram (2012). Laboratory measurements of the O I release rates are required to help settle this discrepancy. It may be possible that the release rates from McKay et al. (2015) are simply effective release rates. The release rates derived using photochemical models might be correct in the strict sense, but perhaps other physical processes occur in the coma (collisional processes, radiative transfer effects, etc.) that modify the [O I] emission so that applying those release rates to remote sensing observations does not reproduce the measured CO₂ abundance of the comet. A more detailed understanding of the coma environment and its effect on [O I] emission is needed.

5 Conclusions

We have presented near-contemporaneous observations of CO₂ using *Spitzer* IRAC and observations of the forbidden oxygen lines in three comets: C/2012 K1 (PanSTARRS), C/2012 K5 (LINEAR), and 290P/Jäger, as well as observations of OH in PanSTARRS and Jäger. Our measured CO₂ abundances are within the spread of values previously observed, corroborating previous observations that the typical CO₂/H₂O ratio in comets is in the range 15-30% and consistent with the theory that CO₂ forms via grain surface reactions involving CO. We find evidence for a possible extended source for H₂O sublimation in PanSTARRS, which we interpret as an icy grain halo, similar to that observed for C/2009 P1 (Garradd). We detected all three forbidden oxygen lines only for PanSTARRS; for the other two comets only the 6300 Å and 6364 Å lines were detected. Therefore for LINEAR and Jäger we only obtained an upper limit on the oxygen line ratio. We compared the CO₂ abundance inferred from the oxygen line ratios to the CO₂ abundance observed by *Spitzer* to evaluate our understanding of the photochemistry responsible for the release of O I into the coma. The upper limits derived for LINEAR and Jäger are not particularly constraining, but we determined that the empirical release rates from McKay et al. (2015) reproduced the CO₂ abundance in PanSTARRS more accurately than the release rates from Bhardwaj and Raghuram (2012). The reason why the empirical release rates seem to reproduce the CO₂ abundance more accurately than those determined from photochemical models like Bhardwaj and Raghuram (2012) is unclear. More work is needed on all fronts, observational, laboratory, and theoretical, to fully understand O I emission in comets and employ it as a reliable proxy for CO₂.

Acknowledgements

We thank two anonymous reviewers whose comments improved the quality of this manuscript. This work was supported by the NASA Planetary Atmospheres Program through grant number NNX08A052G. This work is partially based on observations made with the *Spitzer* Space Telescope, which is operated by the Jet Propulsion Laboratory, California Institute of Technology under a contract with NASA. We thank the APO and Keck observing staff for their invaluable help in conducting the observations. We are thankful to Matthew Knight for productive discussions concerning the coma morphology seen at optical wavelengths for C/2012 K1 (PanSTARRS), as well as David Schleicher, Michael Combi, and Erika Gibb for sharing their unpublished production rates. We thank John Barentine, Jurek Krzesinski, Chris Churchill, Pey Lian Lim, Paul Strycker, and Doug Hoffman for developing and optimizing the ARCES IRAF reduction script used to reduce the ARCES data. We would also like to acknowledge the JPL Horizons System, which was used to generate ephemerides for nonsidereal tracking of the comets during the ARCES observations, and the SIMBAD database, which was used for selection of reference stars. The authors wish to recognize and acknowledge the very significant cultural role and reverence that the summit of Maunakea has always had within the indigenous Hawaiian community. We are most fortunate to have the opportunity to conduct observations from this mountain.

References

- M. F. A'Hearn, M. J. S. Belton, W. A. Delamere, L. M. Feaga, D. Hampton, J. Kissel, K. P. Klaasen, L. A. McFadden, K. J. Meech, H. J. Melosh, P. H. Schultz, J. M. Sunshine, P. C. Thomas, J. Veverka, D. D. Wellnitz, D. K. Yeomans, S. Besse, D. Bodewits, T. J. Bowling, B. T. Carcich, S. M. Collins, T. L. Farnham, O. Groussin, B. Hermalyn, M. S. Kelley, M. S. Kelley, J.-Y. Li, D. J. Lindler, C. M. Lisse, S. A. McLaughlin, F. Merlin, S. Protopapa, J. E. Richardson, and J. L. Williams. EPOXI at Comet Hartley 2. *Science*, 332:1396–, June 2011. doi: 10.1126/science.1204054.
- M. F. A'Hearn, L. M. Feaga, H. U. Keller, H. Kawakita, D. L. Hampton, J. Kissel, K. P. Klaasen, L. A. McFadden, K. J. Meech, P. H. Schultz, J. M. Sunshine, P. C. Thomas, J. Veverka, D. K. Yeomans, S. Besse, D. Bodewits, T. L. Farnham, O. Groussin, M. S. Kelley, C. M. Lisse, F. Merlin, S. Protopapa, and D. D. Wellnitz. Cometary Volatiles and the Origin of Comets. *Astrophysical Journal*, 758:29, October 2012. doi: 10.1088/0004-637X/758/1/29.
- J. M. Bauer, R. G. Walker, A. K. Mainzer, J. R. Masiero, T. Grav, J. W. Dailey, R. S. McMillan, C. M. Lisse, Y. R. Fernández, K. J. Meech, J. Pittichova, E. K. Blauvelt, F. J. Masci, M. F. A'Hearn, R. M. Cutri, J. V. Scotti, D. J. Tholen, E. DeBaun, A. Wilkins, E. Hand, E. L. Wright, and WISE Team. WISE/NEOWISE Observations of Comet 103P/Hartley 2. *Astrophysical Journal*, 738:171, September 2011. doi: 10.1088/0004-637X/738/2/171.
- J. M. Bauer, E. Kramer, A. K. Mainzer, R. Stevenson, T. Grav, J. R. Masiero, R. G. Walker, Y. R. Fernández, K. J. Meech, C. M. Lisse, P. R. Weissman, R. M. Cutri, J. W. Dailey, F. J. Masci, D. J. Tholen, G. Pearman, E. L. Wright, and WISE Team. WISE/NEOWISE Prelim-

- inary Analysis and Highlights of the 67p/Churyumov-Gerasimenko near Nucleus Environs. *Astrophysical Journal*, 758:18, October 2012. doi: 10.1088/0004-637X/758/1/18.
- J. M. Bauer, R. Stevenson, E. Kramer, A. K. Mainzer, T. Grav, J. R. Masiero, Y. R. Fernández, R. M. Cutri, J. W. Dailey, F. J. Masci, K. J. Meech, R. Walker, C. M. Lisse, P. R. Weissman, C. R. Nugent, S. Sonnett, N. Blair, A. Lucas, R. S. McMillan, E. L. Wright, t. WISE, and NEOWISE Teams. The NEOWISE-Discovered Comet Population and the CO+CO₂ production rates. *ArXiv e-prints*, September 2015.
- M. J. S. Belton and J. Melosh. Fluidization and multiphase transport of particulate cometary material as an explanation of the smooth terrains and repetitive outbursts on 9P/Tempel 1. *Icarus*, 200:280–291, March 2009. doi: 10.1016/j.icarus.2008.11.012.
- A. Bhardwaj and S. Raghuram. Model for Cameron-band emission in comets: a case for the EPOXI mission target comet 103P/Hartley 2. *Monthly Notices of the Royal Astronomical Society*, 412:L25–L29, March 2011. doi: 10.1111/j.1745-3933.2010.00998.x.
- A. Bhardwaj and S. Raghuram. A Coupled Chemistry-emission Model for Atomic Oxygen Green and Red-doublet Emissions in the Comet C/1996 B2 Hyakutake. *Astrophysical Journal*, 748:13, March 2012. doi: 10.1088/0004-637X/748/1/13.
- N. Biver, D. Bockelée-Morvan, P. Colom, J. Crovisier, F. Henry, E. Lellouch, A. Winnberg, L.E.B. Johansson, M. Gunnarsson, H. Rickman, F. Rantakyö, Davies. J.K., W.R.F. Dent, G. Paubert, R. Moreno, J. Wink, D. Despois, D. Benford, M. Gardner, D.C. Lis, D. Mehringer, T.G. Phillips, and H. Rauer. The 1995-2002 long-term monitoring of comet C/1995 O1 (Hale-Bopp) at radio wavelength. *Earth, Moon, and Planets*, 90(1):5–14,

2002.

D. Bodewits, T. L. Farnham, M. F. A'Hearn, L. M. Feaga, A. McKay, D. G. Schleicher, and J. M. Sunshine. The Evolving Activity of the Dynamically Young Comet C/2009 P1 (Garradd). *Astrophysical Journal*, 786:48, May 2014. doi: 10.1088/0004-637X/786/1/48.

M.T. Capria, G. Cremonese, A. Bhardwaj, and M.C. de Sanctis. O¹S and O¹D emission lines in the spectrum of 153P/2002 C1 (Ikeya-Zhang). *Astronomy and Astrophysics*, 442(3):1121–1126, 2005.

A. L. Cochran and D. G. Schleicher. Observational Constraints on the Lifetime of Cometary H₂O. *Icarus*, 105:235–253, September 1993. doi: 10.1006/icar.1993.1121.

A.L. Cochran. Atomic oxygen in the comae of comets. *Icarus*, 198(1):181–188, 2008.

A.L. Cochran and W.D. Cochran. Observations of O (¹S) and O (¹D) in spectra of C/1999 S4 (LINEAR). *Icarus*, 154(2):381–390, 2001.

M. Combes, J. Crovisier, T. Encrenaz, V. I. Moroz, and J.-P. Bibring. The 2.5-12 micron spectrum of Comet Halley from the IKS-VEGA Experiment. *Icarus*, 76:404–436, December 1988. doi: 10.1016/0019-1035(88)90013-9.

M. Combi, W. Harris, and W. Smyth. Gas dynamics and kinetics in the cometary coma: Theory and observations. In *Comets II*, pages 523–552, Tucson, AZ, USA, 2004. University of Arizona Press.

M. R. Combi, J. T. T. Mäkinen, J.-L. Bertaux, E. Quémerais, S. Ferron, and N. Fougere. Water production rate of Comet C/2009 P1 (Garradd) throughout the 2011-2012 apparition: Evidence for an icy grain halo. *Icarus*, 225:740–748, July 2013. doi: 10.1016/j.icarus.2013.04.030.

M. R. Combi, J. T. Mäkinen, J. L. Bertaux, E. Quémerais, and S. Ferron. The Water Production Rate of Recent Comets (2013-2014) by SOHO/SWAN:

- 2P/Encke (2013), C/2013 R1 (Lovejoy), and C/2013 A1 (Siding Spring). In *AAS/Division for Planetary Sciences Meeting Abstracts*, volume 46 of *AAS/Division for Planetary Sciences Meeting Abstracts*, page 110.09, November 2014.
- J. Crovisier. Infrared observations of volatile molecules in comet Hale-Bopp. *Earth, Moon, and Planets*, 79(1/3):125–143, 1997.
- J. Crovisier and T. Encrenaz. Infrared fluorescence of molecules in comets - The general synthetic spectrum. *Astronomy and Astrophysics*, 126:170–182, September 1983.
- A. Decock, E. Jehin, D. Hutsemékers, and J. Manfroid. Forbidden oxygen lines in comets at various heliocentric distances. *Astronomy and Astrophysics*, 555:A34, July 2013. doi: 10.1051/0004-6361/201220414.
- A. Decock, E. Jehin, P. Rousselot, D. Hutsemékers, J. Manfroid, S. Raghuram, A. Bhardwaj, and B. Hubert. Forbidden oxygen lines at various nucleocentric distances in comets. *Astronomy and Astrophysics*, 573:A1, January 2015. doi: 10.1051/0004-6361/201424403.
- M. A. DiSanti, G. L. Villanueva, L. Paganini, B. P. Bonev, J. V. Keane, K. J. Meech, and M. J. Mumma. Pre- and post-perihelion observations of C/2009 P1 (Garradd): Evidence for an oxygen-rich heritage? *Icarus*, 228:167–180, January 2014. doi: 10.1016/j.icarus.2013.09.001.
- G. G. Fazio, J. L. Hora, L. E. Allen, M. L. N. Ashby, P. Barmby, L. K. Deutsch, J.-S. Huang, S. Kleiner, M. Marengo, S. T. Megeath, G. J. Melnick, M. A. Pahre, B. M. Patten, J. Polizotti, H. A. Smith, R. S. Taylor, Z. Wang, S. P. Willner, W. F. Hoffmann, J. L. Pipher, W. J. Forrest, C. W. McMurty, C. R. McCreight, M. E. McKelvey, R. E. McMurray, D. G. Koch, S. H. Moseley, R. G. Arendt, J. E. Mentzell, C. T. Marx, P. Losch, P. Mayman, W. Eichhorn, D. Krebs, M. Jhabvala, D. Y. Gezari, D. J. Fixsen, J. Flores,

- K. Shakoorzadeh, R. Jungo, C. Hakun, L. Workman, G. Karpati, R. Kichak, R. Whitley, S. Mann, E. V. Tollestrup, P. Eisenhardt, D. Stern, V. Gorjian, B. Bhattacharya, S. Carey, B. O. Nelson, W. J. Glaccum, M. Lacy, P. J. Lowrance, S. Laine, W. T. Reach, J. A. Stauffer, J. A. Surace, G. Wilson, E. L. Wright, A. Hoffman, G. Domingo, and M. Cohen. The Infrared Array Camera (IRAC) for the Spitzer Space Telescope. *Astrophysical Journal Supplement Series*, 154:10–17, September 2004. doi: 10.1086/422843.
- L. M. Feaga, M. F. A’Hearn, T. L. Farnham, D. Bodewits, J. M. Sunshine, A. M. Gersch, S. Protopapa, B. Yang, M. Drahus, and D. G. Schleicher. Uncorrelated Volatile Behavior during the 2011 Apparition of Comet C/2009 P1 Garradd. *Astronomical Journal*, 147:24, January 2014. doi: 10.1088/0004-6256/147/1/24.
- L.M. Feaga, M.F. A’Hearn, J.M. Sunshine, O. Groussin, and T.L. Farnham. Asymmetries in the distribution of H₂O and CO₂ in the inner coma of comet 9P/Tempel 1 as observed by Deep Impact. *Icarus*, 190(2):345–356, 2007.
- M.C. Festou. The density distribution of neutral compounds in cometary atmospheres I - models and equations. *Astronomy and Astrophysics*, 95(1): 69–79, 1981.
- R. T. Garrod and T. Pauly. On the Formation of CO₂ and Other Interstellar Ices. *Astrophysical Journal*, 735:15, July 2011. doi: 10.1088/0004-637X/735/1/15.
- N. Gehrels, G. Chincarini, P. Giommi, K. O. Mason, J. A. Nousek, A. A. Wells, N. E. White, S. D. Barthelmy, D. N. Burrows, L. R. Cominsky, K. C. Hurley, F. E. Marshall, P. Mészáros, P. W. A. Roming, L. Angelini, L. M. Barbier, T. Belloni, S. Campana, P. A. Caraveo, M. M. Chester, O. Citterio, T. L. Cline, M. S. Cropper, J. R. Cummings, A. J. Dean, E. D. Feigelson, E. E. Fenimore, D. A. Frail, A. S. Fruchter, G. P. Garmire, K. Gendreau, G. Ghis-

- ellini, J. Greiner, J. E. Hill, S. D. Hunsberger, H. A. Krimm, S. R. Kulka-
rni, P. Kumar, F. Lebrun, N. M. Lloyd-Ronning, C. B. Markwardt, B. J.
Mattson, R. F. Mushotzky, J. P. Norris, J. Osborne, B. Paczynski, D. M.
Palmer, H.-S. Park, A. M. Parsons, J. Paul, M. J. Rees, C. S. Reynolds,
J. E. Rhoads, T. P. Sasseen, B. E. Schaefer, A. T. Short, A. P. Smale, I. A.
Smith, L. Stella, G. Tagliaferri, T. Takahashi, M. Tashiro, L. K. Townsley,
J. Tueller, M. J. L. Turner, M. Vietri, W. Voges, M. J. Ward, R. Willingale,
F. M. Zerbi, and W. W. Zhang. The Swift Gamma-Ray Burst Mission.
Astrophysical Journal, 611:1005–1020, August 2004. doi: 10.1086/422091.
- M. S. P. Kelley, C. E. Woodward, D. Bodewits, T. L. Farnham, M. Gudipati,
D. E. Harker, D. C. Hines, M. M. Knight, L. Kolokolova, A. Li, I. de Pater,
S. Protopapa, R. W. Russell, and Wooden D. W. Sitko, M. L. Cometary
Science with the James Webb Space Telescope. submitted, 2015.
- M. M. Knight and D. G. Schleicher. Coma Morphology of Recent Comets:
C/ISON (2012 S1), C/Pan-STARRS (2012 K1), C/Jacques (2014 E2), and
C/Siding Spring (2013 A1). In *AAS/Division for Planetary Sciences Meet-
ing Abstracts*, volume 46 of *AAS/Division for Planetary Sciences Meeting
Abstracts*, page 209.20, November 2014.
- S. Laine, editor. *IRAC Instrument Handbook*.
Spitzer Science Center, Pasadena, 2015. URL
<http://irsa.ipac.caltech.edu/data/SPITZER/docs/irac/iracinstrumenthandbook/>.
- D. Makovoz and I. Khan. Mosaicking with MOPEX. In P. Shopbell, M. Brit-
ton, and R. Ebert, editors, *Astronomical Data Analysis Software and Sys-
tems XIV*, volume 347 of *Astronomical Society of the Pacific Conference
Series*, page 81, December 2005.
- K. O. Mason, A. Breeveld, S. D. Hunsberger, C. James, T. E. Kennedy,
P. W. A. Roming, and J. Stock. Performance of the UV/Optical Telescope

- (UVOT) on SWIFT. In K. A. Flanagan and O. H. W. Siegmund, editors, *X-Ray and Gamma-Ray Instrumentation for Astronomy XIII*, volume 5165 of *Society of Photo-Optical Instrumentation Engineers (SPIE) Conference Series*, pages 277–286, February 2004. doi: 10.1117/12.503713.
- A. J. McKay, N. J. Chanover, J. P. Morgenthaler, A. L. Cochran, W. M. Harris, and N. D. Russo. Forbidden oxygen lines in Comets C/2006 W3 Christensen and C/2007 Q3 Siding Spring at large heliocentric distance: Implications for the sublimation of volatile ices. *Icarus*, 220:277–285, July 2012. doi: 10.1016/j.icarus.2012.04.030.
- A. J. McKay, N. J. Chanover, J. P. Morgenthaler, A. L. Cochran, W. M. Harris, and N. D. Russo. Observations of the forbidden oxygen lines in DIXI target Comet 103P/Hartley. *Icarus*, 222:684–690, February 2013. doi: 10.1016/j.icarus.2012.06.020.
- A. J. McKay, N. J. Chanover, M. A. DiSanti, J. P. Morgenthaler, A. L. Cochran, W. M. Harris, and N. D. Russo. Rotational variation of daughter species production rates in Comet 103P/Hartley: Implications for the progeny of daughter species and the degree of chemical heterogeneity. *Icarus*, 231:193–205, March 2014. doi: 10.1016/j.icarus.2013.11.029.
- A. J. McKay, A. L. Cochran, M. A. DiSanti, G. Villanueva, N. D. Russo, R. J. Vervack, J. P. Morgenthaler, W. M. Harris, and N. J. Chanover. Evolution of H₂O, CO, and CO₂ production in Comet C/2009 P1 Garradd during the 2011-2012 apparition. *Icarus*, 250:504–515, April 2015. doi: 10.1016/j.icarus.2014.12.023.
- K. Meech and J. Svoren. Physical and chemical evolution of cometary nuclei. In *Comets II*, pages 317–335, Tucson, AZ, USA, 2004. University of Arizona Press.
- M. Minissale, E. Congiu, G. Manicò, V. Pirronello, and F. Dulieu. CO₂ for-

- mation on interstellar dust grains: a detailed study of the barrier of the CO + O channel. *Astronomy and Astrophysics*, 559:A49, November 2013. doi: 10.1051/0004-6361/201321453.
- J.P. Morgenthaler, W.M. Harris, and M.R. Combi. Large Aperture O I 6300 Å Observations of Comet Hyakutake: Implications for the Photochemistry of OH and O I Production in Comet Hale-Bopp. *Astrophysical Journal*, 657: 1162–1171, March 2007. doi: 10.1086/511062.
- M. J. Mumma and S. B. Charnley. The Chemical Composition of Comets - Emerging Taxonomies and Natal Heritage. *Annual Review of Astronomy and Astrophysics*, 49:471–524, September 2011. doi: 10.1146/annurev-astro-081309-130811.
- J. A. Noble, F. Dulieu, E. Congiu, and H. J. Fraser. CO₂ Formation in Quiescent Clouds: An Experimental Study of the CO + OH Pathway. *Astrophysical Journal*, 735:121, July 2011. doi: 10.1088/0004-637X/735/2/121.
- T. Ootsubo, F. Usui, H. Kawakita, M. Ishiguro, R. Furusho, S. Hasegawa, M. Ueno, J.-i. Watanabe, T. Sekiguchi, T. Wada, Y. Ohyama, S. Oyabu, H. Matsuhara, T. Onaka, T. Nakagawa, and H. Murakami. Detection of Parent H₂O and CO₂ Molecules in the 2.5-5 μm Spectrum of Comet C/2007 N3 (Lulin) Observed with AKARI. *Astrophysical Journal Letters*, 717:L66–L70, July 2010. doi: 10.1088/2041-8205/717/1/L66.
- T. Ootsubo, H. Kawakita, S. Hamada, H. Kobayashi, M. Yamaguchi, F. Usui, T. Nakagawa, M. Ueno, M. Ishiguro, T. Sekiguchi, J.-i. Watanabe, I. Sakon, T. Shimonishi, and T. Onaka. AKARI Near-infrared Spectroscopic Survey for CO₂ in 18 Comets. *Astrophysical Journal*, 752:15, June 2012. doi: 10.1088/0004-637X/752/1/15.
- J. Pittichová, C. E. Woodward, M. S. Kelley, and W. T. Reach. Ground-Based Optical and Spitzer Infrared Imaging Observations of Comet

- 21P/GIACOBINI-ZINNER. *Astronomical Journal*, 136:1127–1136, September 2008. doi: 10.1088/0004-6256/136/3/1127.
- S. Raghuram and A. Bhardwaj. Photochemistry of atomic oxygen green and red-doublet emissions in comets at larger heliocentric distances. *Astronomy and Astrophysics*, 566:A134, June 2014. doi: 10.1051/0004-6361/201321921.
- W. T. Reach, J. Vaubaillon, M. S. Kelley, C. M. Lisse, and M. V. Sykes. Distribution and properties of fragments and debris from the split Comet 73P/Schwassmann-Wachmann 3 as revealed by Spitzer Space Telescope. *Icarus*, 203:571–588, October 2009. doi: 10.1016/j.icarus.2009.05.027.
- W. T. Reach, M. S. Kelley, and J. Vaubaillon. Survey of cometary CO₂, CO, and particulate emissions using the Spitzer Space Telescope. *Icarus*, 226: 777–797, September 2013. doi: 10.1016/j.icarus.2013.06.011.
- P. W. A. Roming, T. E. Kennedy, K. O. Mason, J. A. Nousek, L. Ahr, R. E. Bingham, P. S. Broos, M. J. Carter, B. K. Hancock, H. E. Huckle, S. D. Hunsberger, H. Kawakami, R. Killough, T. S. Koch, M. K. McLelland, K. Smith, P. J. Smith, J. C. Soto, P. T. Boyd, A. A. Breeveld, S. T. Holland, M. Ivanushkina, M. S. Pryzby, M. D. Still, and J. Stock. The Swift Ultra-Violet/Optical Telescope. *Space Science Reviews*, 120:95–142, October 2005. doi: 10.1007/s11214-005-5095-4.
- D. G. Schleicher and M. F. A’Hearn. The fluorescence of cometary OH. *Astrophysical Journal*, 331:1058–1077, August 1988. doi: 10.1086/166622.
- BD Sharpee and TG Slinger. O (1d2-3p2, 1, 0) 630.0, 636.4, and 639.2 nm forbidden emission line intensity ratios measured in the terrestrial nightglow. *The Journal of Physical Chemistry A*, 110(21):6707–6710, 2006.
- R. Stevenson, J. M. Bauer, R. M. Cutri, A. K. Mainzer, and F. J. Masci. NEOWISE Observations of Comet C/2013 A1 (Siding Spring) as It Approaches Mars. *Astrophysical Journal Letters*, 798:L31, January 2015. doi:

10.1088/2041-8205/798/2/L31.

- W.-L. Tseng, D. Bockelée-Morvan, J. Crovisier, P. Colom, and W.-H. Ip. Cometary water expansion velocity from OH line shapes. *Astronomy and Astrophysics*, 467:729–735, May 2007. doi: 10.1051/0004-6361:200666666.
- S. S. Vogt, S. L. Allen, B. C. Bigelow, L. Bresee, B. Brown, T. Cantrall, A. Conrad, M. Couture, C. Delaney, H. W. Epps, D. Hilyard, D. F. Hilyard, E. Horn, N. Jern, D. Kanto, M. J. Keane, R. I. Kibrick, J. W. Lewis, J. Osborne, G. H. Pardeilhan, T. Pfister, T. Ricketts, L. B. Robinson, R. J. Stover, D. Tucker, J. Ward, and M. Z. Wei. HIRES: the high-resolution echelle spectrometer on the Keck 10-m Telescope. In D. L. Crawford and E. R. Craine, editors, *Instrumentation in Astronomy VIII*, volume 2198 of *Society of Photo-Optical Instrumentation Engineers (SPIE) Conference Series*, page 362, June 1994.
- S.-i. Wang, R. H. Hildebrand, L. M. Hobbs, S. J. Heimsath, G. Kelderhouse, R. F. Loewenstein, S. Lucero, C. M. Rockosi, D. Sandford, J. L. Sundwall, J. A. Thorburn, and D. G. York. ARCES: an echelle spectrograph for the Astrophysical Research Consortium (ARC) 3.5m telescope. In M. Iye and A. F. M. Moorwood, editors, *Instrument Design and Performance for Optical/Infrared Ground-based Telescopes*, volume 4841 of *Society of Photo-Optical Instrumentation Engineers (SPIE) Conference Series*, pages 1145–1156, March 2003. doi: 10.1117/12.461447.
- H.A. Weaver, P.D. Feldman, J.B. McPhate, M.F. A’Hearn, C. Arpigny, and T.E. Smith. Detection of CO Cameron band emission in comet P/Hartley 2 (1991 XV). *Astrophysical Journal*, 422(1):374–380, 1994.
- M. W. Werner, T. L. Roellig, F. J. Low, G. H. Rieke, M. Rieke, W. F. Hoffmann, E. Young, J. R. Houck, B. Brandl, G. G. Fazio, J. L. Hora, R. D. Gehrz, G. Helou, B. T. Soifer, J. Stauffer, J. Keene, P. Eisenhardt, D. Gal-

lagher, T. N. Gautier, W. Irace, C. R. Lawrence, L. Simmons, J. E. Van
Cleve, M. Jura, E. L. Wright, and D. P. Cruikshank. The Spitzer Space Tele-
scope Mission. *Astrophysical Journal Supplement Series*, 154:1–9, Septem-
ber 2004. doi: 10.1086/422992.

Table 1

Observation Log-*Spitzer*

Comet	Date (UT)	R (AU)	Δ^a (AU)	Exp. Times (s)	Effective On-Source Exp. Time (s)
LINEAR	1/31/2013	1.51	1.03	1.2 and 30	236
LINEAR	2/15/2013	1.66	1.04	0.6, 12, and 100	936
Jäger	2/3/2014	2.18	1.81	0.6, 12, and 100	562
PanSTARRS	5/25/2014	1.83	1.24	0.6 and 6	26.4

a Distance from *Spitzer*

Table 2

Observation Log-APO/Keck

Comet	Date (UT)	r (AU)	Δ (AU)	$\dot{\Delta}$ (km s ⁻¹)	G2V	Fast Rot.	Flux Cal
LINEAR	2/7/2013	1.57	1.11	47.0	HD 25370	HD 27660	HR 1544
LINEAR	2/15/2013	1.66	1.35	46.2	HD 25370	HD 27660	HR 1544
Jäger	11/6/2013	2.45	1.78	-23.7	HD 259216	HR 2532	Hilt 600
Jäger	11/15/2013	2.42	1.66	-21.7	HD 259516	HR 2532	Hilt 600
Jäger ^a	1/14/2014	2.22	1.28	1.8	Hyades 64	HR 2207	Hilt 600
PanSTARRS	6/4/2014	1.71	1.69	19.5	35 Leo	33 LMi	HD 93521

^a Obtained with Keck HIRES

Table 3

Observed Fluxes

Comet	Date (UT)	Species	Flux ^a	3.6 μm Scale Factor ^b
LINEAR	1/31/2013	CO ₂	1.31 \pm 0.36	3.25 \pm 0.12
LINEAR	2/15/2013	CO ₂	0.89 \pm 0.18	2.59 \pm 0.71
Jäger	2/3/2014	CO ₂	1.55 \pm 0.15	1.63 \pm 0.24
PanSTARRS	5/25/2014	CO ₂	38.8 \pm 0.1	1.69 \pm 0.01
LINEAR	2/7/2013	[O I]	0.39 \pm 0.04	-
LINEAR	2/15/2013	[O I]	0.30 \pm 0.04	-
Jäger	11/6/2013	[O I]	0.22 \pm 0.03	-
Jäger	11/15/2013	[O I]	0.33 \pm 0.05	-
PanSTARRS	6/4/2014	[O I]	23.8 \pm 2.5	-
Jäger	1/14/2014	OH	5.97 \pm 0.6	-
PanSTARRS	5/7/2014	OH	63500 \pm 60	-

^a Fluxes are in 10^{-15} ergs s⁻¹ cm⁻². For CO₂ *Spitzer* observations, fluxes are for a 33-pixel aperture. For *Swift* OH observations, flux is given for a 50-pixel aperture. For [O I] and OH from ARCES and HIRES, fluxes are integrated over the entire slit.

^b Only applicable to *Spitzer* observations of CO₂.

Table 4

Production Rates, CO₂/H₂O Ratios, and Collisional Quenching Factors

Comet	Q (10^{26} mol s ⁻¹)				
	R (AU)	CO ₂	H ₂ O	CO ₂ /H ₂ O (%)	Coll. Quench. Factor
PanSTARRS	1.83	54.6 ± 0.1	435 ± 44 ^a	12.6 ± 1.3	1.25
PanSTARRS ^b	2.04	-	950 ± 80	-	-
LINEAR	1.51	1.12 ± 0.08 ^c	3.88 ± 0.4	28.9 ± 3.6 ^c	1.03
Jäger ^d	2.42	4.23 ± 0.37	13.5 ± 1.4	31.3 ± 4.2	-
Jäger ^e	2.18	-	10.2 ± 1.5	-	1.00

^a H₂O Production from ARCES observations of [O I] emission.

^b H₂O Production from *Swift* observations of OH.

^c Due to uncertainties associated with the model-dependent dust subtraction, these values may be better interpreted as upper limits.

^d Q_{H_2O} from January Keck HIRES observations of OH, no collisional quenching factor is given due to no O I observation being obtained at this epoch.

^e Q_{H_2O} from November ARCES observations of [O I]6300 emission. Q_{CO_2} is not provided as the *Spitzer* observation was in early February, therefore a comparison to the H₂O production rate from November is not necessarily meaningful.

Table 5

Inferred vs. Measured CO₂/H₂O Ratio

Comet	O I Ratio	CO ₂ /H ₂ O (%)			
		BR12	McKay2015A	McKay2015B	<i>Spitzer</i>
PanSTARRS	0.054 ± 0.002	3.7 ± 0.3	9.5 ± 0.4	14.4 ± 0.6	12.6 ± 1.3
LINEAR	< 0.169	< 27	< 42	< 64	28.9 ± 3.6
Jäger	< 0.247	< 53	< 77	< 116	31.3 ± 4.2

Table 6

O I Release Rates

Parent	O I State ^a	Release Rates (10^{-8} s^{-1})		
		McKay2015A	McKay2015B	BR2012
H ₂ O	¹ S	0.64	0.64	2.6
H ₂ O	¹ D	84.4	84.4	84.4
CO ₂	¹ S	50.0	33.0	72.0
CO ₂	¹ D	75.0	49.5	120.0
CO	¹ S	4.0	4.0	4.0
CO	¹ D	5.1	5.1	5.1

^a These rates are for a given electron state, not the line. Therefore if not all lines coming from that state are observed, the branching ratio needs to be accounted for. For ¹D, both the 6300 Å and 6364 Å lines are usually observed, so no correction is needed. However, for ¹S, typically only the 5577 Å line is observed (as is the case in this work), so the above rates need to be multiplied by a branching ratio of 0.9 to get the yield for ¹S atoms that will decay through the 5577 Å line.

Figure Captions

Fig 1: Spectrum of Jäger taken with Keck HIRES showing part of the $\Delta v=0$ OH band. The background is due to the effect of scattered moonlight.

Fig 2: *Spitzer* IRAC images at 3.6 (left column) and 4.5 (right column) μm of PanSTARRS (top row), LINEAR (middle row), and Jäger (bottom row). The solar and velocity directions are indicated by the arrows labeled “Sun” and “v”, respectively, while celestial north is depicted by the arrow labeled “N”. It is apparent in the 4.5 μm image of PanSTARRS that there is diffuse emission not present in the 3.6 μm image, which is likely due to CO₂. There appears to be some diffuse emission in the 4.5 μm image of Jäger as well, though it is not as obvious as for PanSTARRS. The gas emission is not obvious in the 4.5 μm image of LINEAR.

Fig 3: Dust-subtracted images of PanSTARRS (top), LINEAR (middle), and Jäger (bottom). The solar and velocity directions are indicated by the arrows labeled “Sun” and “v”, respectively, while celestial north is depicted by the arrow labeled “N”.

Fig 4: *Spitzer* images of PanSTARRS before (top row) and after (bottom row) division by a $1/\rho$ profile. Left to right is 3.6 μm , 4.5 μm , and the dust-subtracted image. The tail is obvious in the 3.6 μm and 4.5 μm images, and a faint residual is still evident in the dust-subtracted image. The dust-subtracted and 4.5 μm images show a spiral structure that is not evident at 3.6 μm , which is likely the manifestation of a CO₂ jet. Each subpanel has dimensions of 220,000 km on a side.

Fig 5: *Spitzer* images of LINEAR before (top row) and after (bottom row) division by a $1/\rho$ profile. Left to right is $3.6 \mu\text{m}$, $4.5 \mu\text{m}$, and the dust-subtracted image. The tail is obvious in the $3.6 \mu\text{m}$ and $4.5 \mu\text{m}$ images, and a faint residual is still evident in the dust-subtracted image. In all images the coma morphology is symmetric, showing no obvious structures. Each subpanel has dimensions of 140,000 km on a side.

Fig 6: *Spitzer* images of Jäger before (top row) and after (bottom row) division by a $1/\rho$ profile. Left to right is $3.6 \mu\text{m}$, $4.5 \mu\text{m}$, and the dust-subtracted image. The tail is obvious in the $3.6 \mu\text{m}$ and $4.5 \mu\text{m}$ images, and a faint residual is still evident in the dust-subtracted image. There is some possible extension of flux toward the bottom of the frame in the dust-subtracted image, but otherwise no coma features are present. Each subpanel has dimensions of 240,000 km on a side.

Fig 7: Spectrum of PanSTARRS depicting the [O I]5577 Å line. The cometary line is redshifted compared to the telluric line and is significantly weaker in intensity.

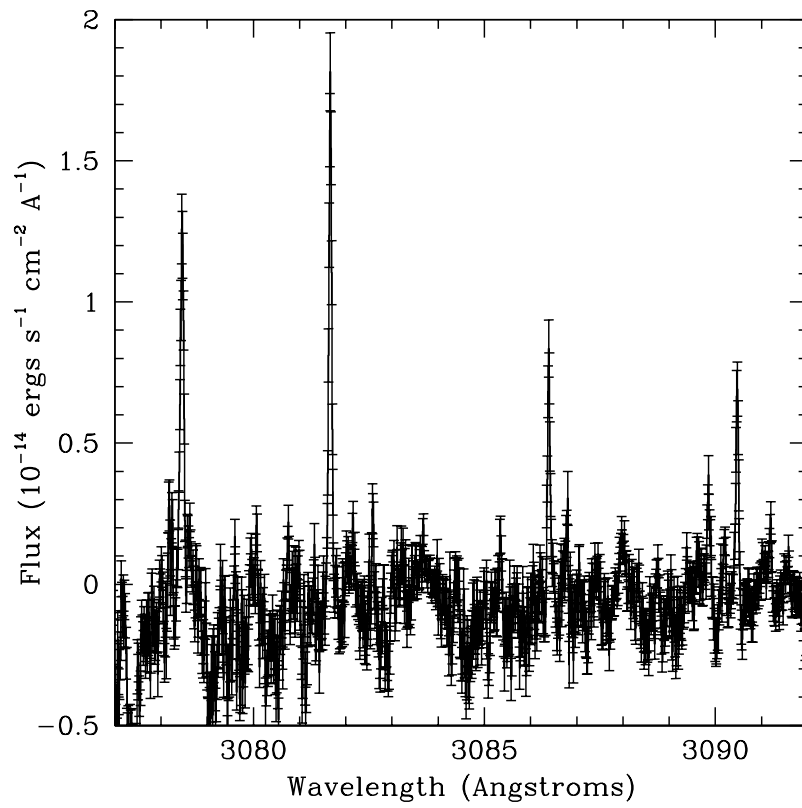


Fig. 1.

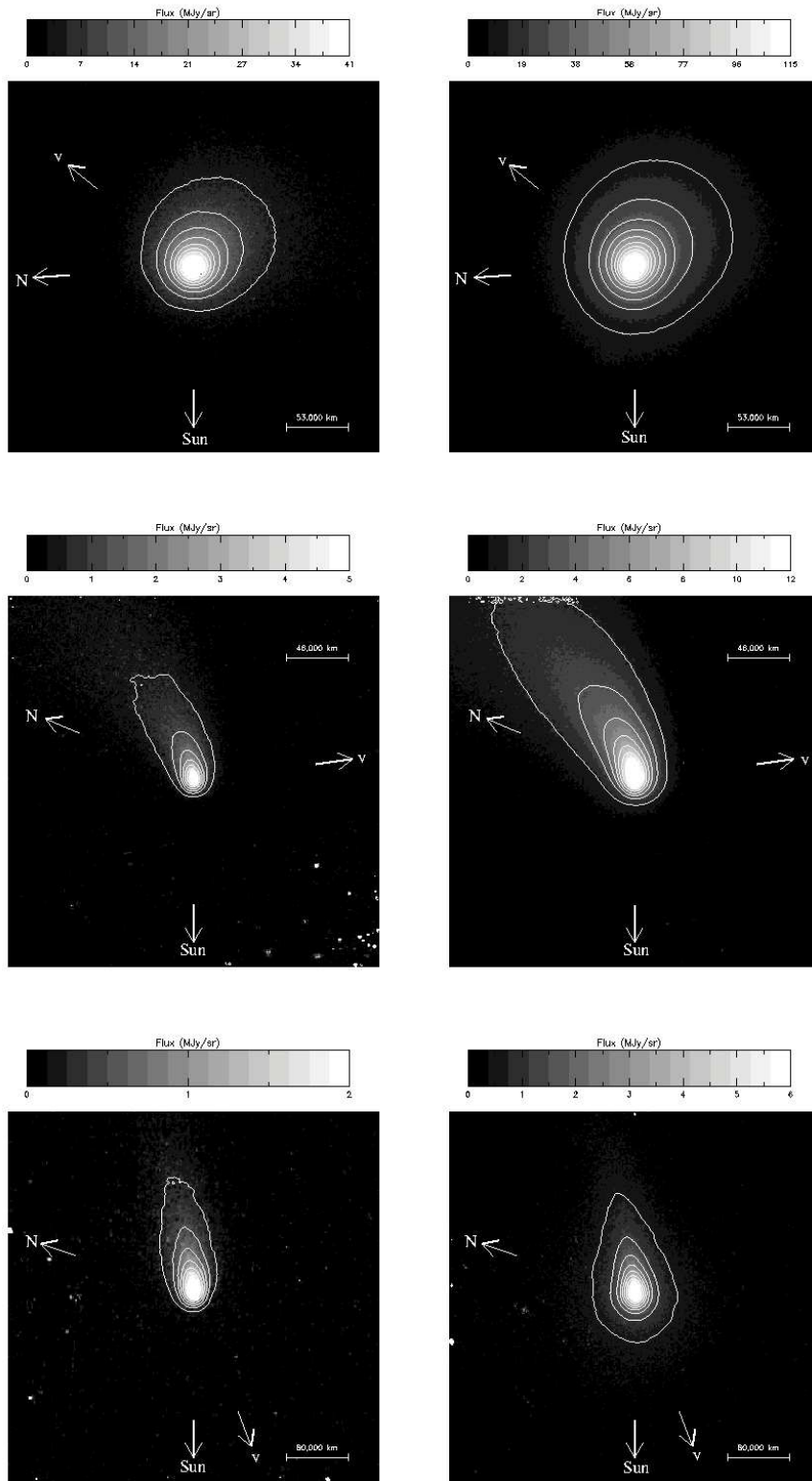


Fig. 2.

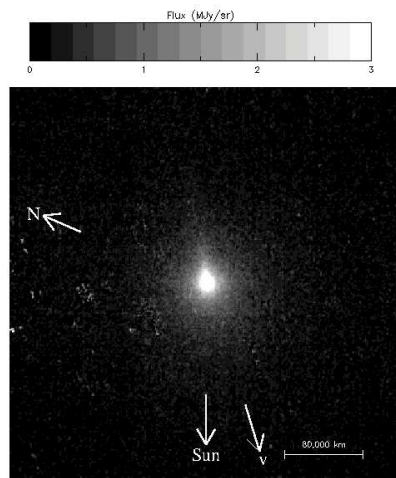
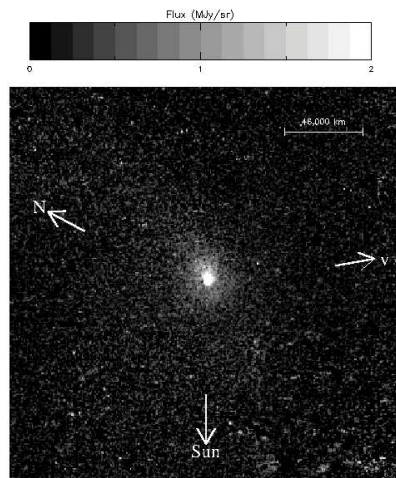
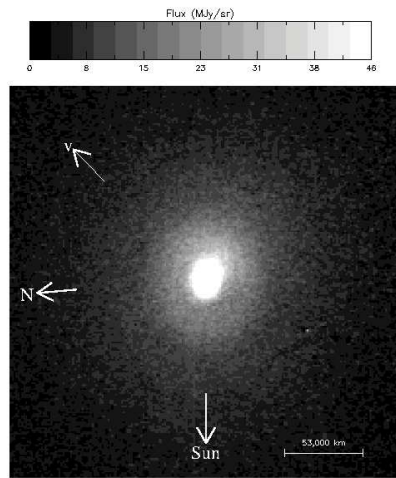


Fig. 3.

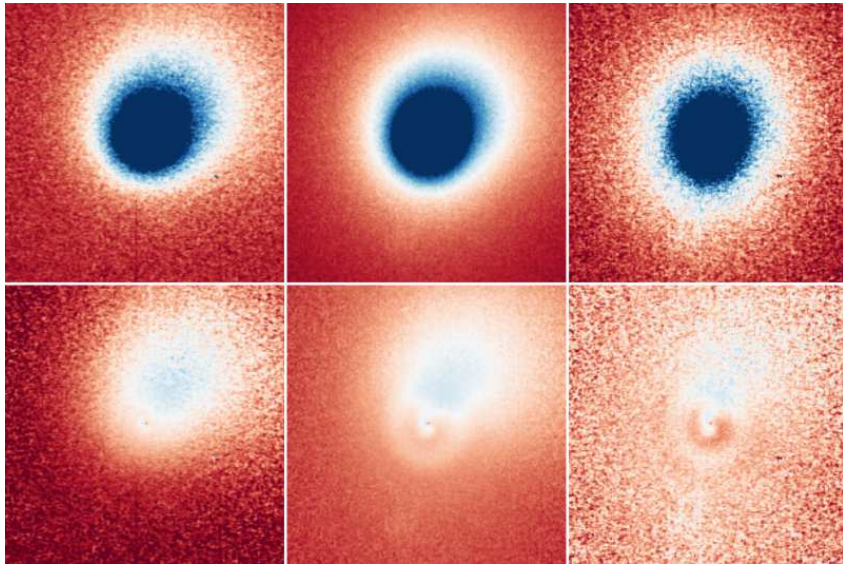


Fig. 4.

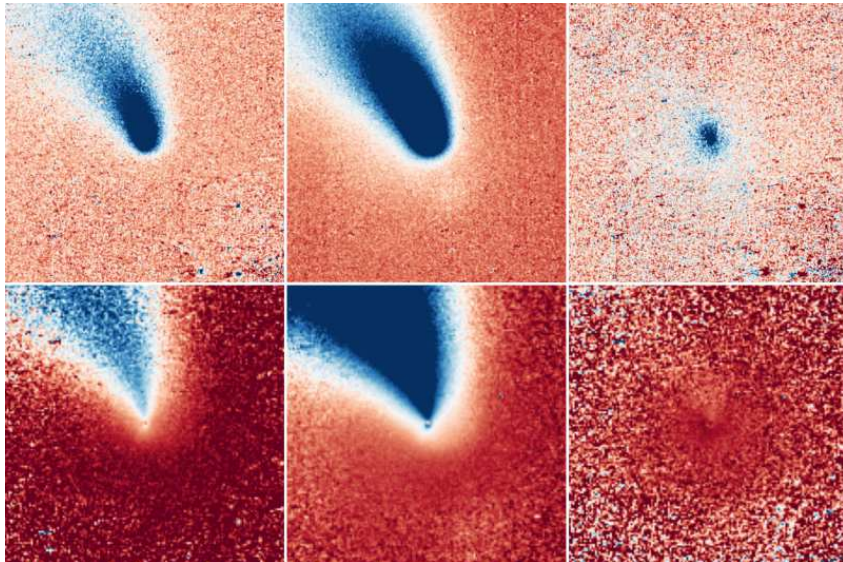


Fig. 5.

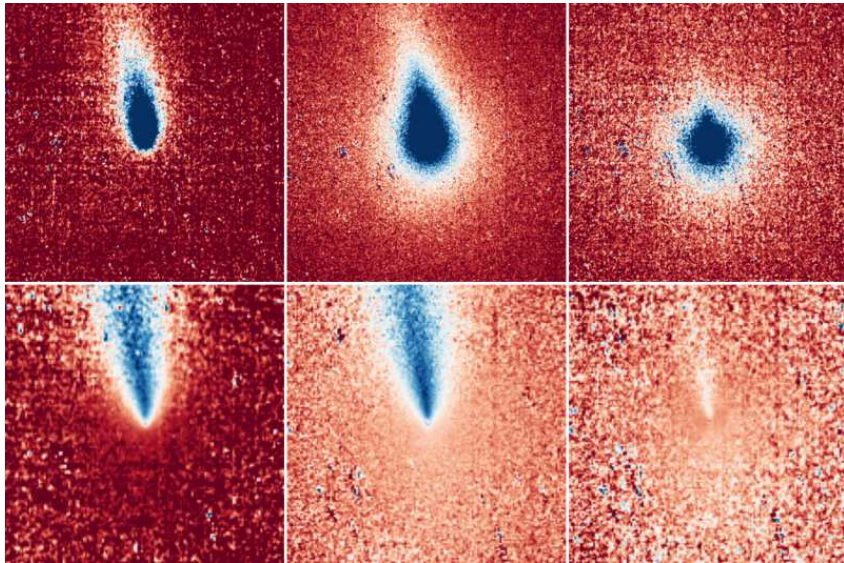


Fig. 6.

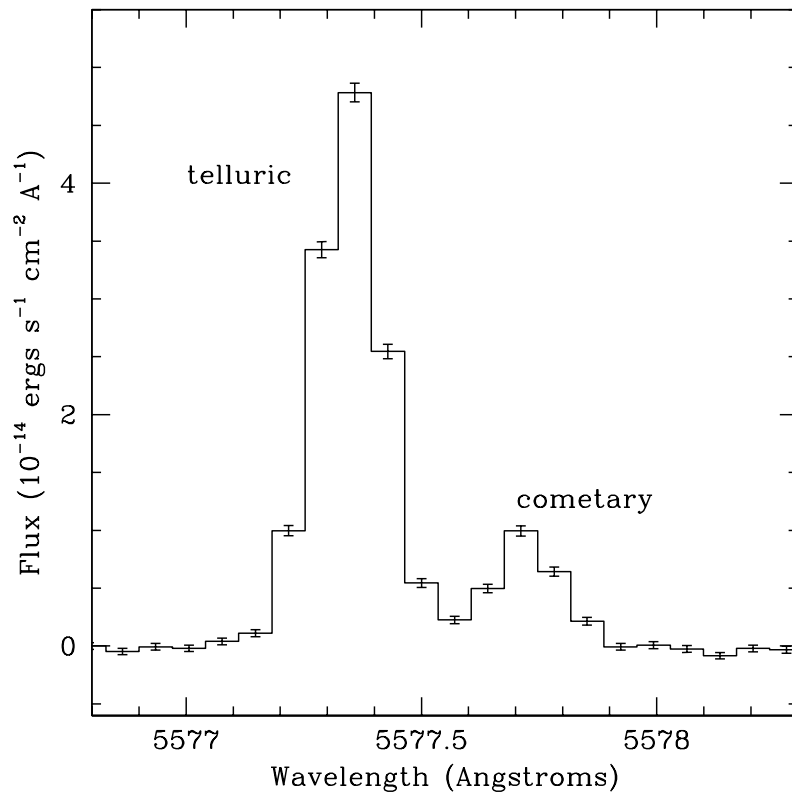


Fig. 7.